The Time-Dependent Response of Atlantic Tropical Cyclone Potential Intensity to Pacific SST Forcing. Part I: A Conceptual Framework

JONATHAN LIN,[a] RAPHAEL ROUSSEAU-RIZZI,[b,c] AND KERRY EMANUEL[d]

[a] *Department of Earth and Atmospheric Sciences, Cornell University, Ithaca, New York*
[b] *Hydro-Quebec Research Center, Varennes, Quebec, Canada*
[c] *Department of Atmospheric and Oceanic Sciences, McGill University, Montreal, Quebec, Canada*
[d] *Lorenz Center, Department of Earth, Atmospheric, and Planetary Sciences, Massachusetts Institute of Technology, Cambridge, Massachusetts*

(Manuscript received 11 September 2025, in final form 19 February 2026, accepted 17 March 2026)

ABSTRACT: Constraining future changes to Atlantic tropical cyclone activity remains challenging, in part because these changes may be sensitive to patterns of warming in the equatorial Pacific. This study examines the time-dependent potential intensity response of the Atlantic to Pacific sea surface temperature (SST) forcing. Using a "double column" model framework under weak-temperature-gradient dynamics, it is shown that the transient response of Atlantic potential intensity to Pacific SST forcing is opposite in sign to the equilibrium response. The time scale that separates the transient and equilibrium responses is found to be proportional to the ocean mixed layer depth, consistent with earlier work. A previously derived linearized potential intensity framework is then used to accurately reproduce the modeled Atlantic potential intensity response, showing that it can be largely understood as a competition between the local surface temperature and the tropically averaged tropospheric temperature. The linear framework is next used to derive a time-dependent linear model that accurately reproduces the behavior of the double-column model. Using analytic solutions to this time-dependent linear model, it is shown that the time evolution of Pacific SST, as opposed to its instantaneous state, more strongly influences Atlantic potential intensity. The difference in sign between the transient and equilibrium potential intensity responses to Pacific SST forcing brings into question the applicability of using the El Niño–Southern Oscillation (ENSO)–Atlantic tropical cyclone relationship to understand the response of Atlantic tropical cyclone activity to long-term warming trends that project onto ENSO.

KEYWORDS: Atmosphere-ocean interaction; Climate; ENSO; Tropical cyclones; Climate change

1. Introduction

Tropical cyclones, characterized by powerful winds, intense rainfall, and life-threatening storm surge, are among the most devastating natural phenomena, often leading to extreme flooding and widespread damage in affected regions. These storms are responsible for billions of dollars of damage per year across the globe, as well as for the loss of life (Zhang et al. 2009; Mendelsohn et al. 2012). In the future, we expect tropical cyclones to intensify, in part because the potential intensity, a thermodynamically based theoretical upper bound on tropical cyclone wind speed, increases with CO_2 emissions (Emanuel 1987). It follows that the hazards and risks associated with tropical cyclones will generally worsen in the future (Knutson et al. 2020; Balaguru et al. 2023; Sarhadi et al. 2024, among many).

While the metrics we use to understand tropical cyclone activity under a variety of climates are generally aggregated on the global scale (Knutson et al. 2020; Emanuel 2021), the societal impacts of these storms are usually felt in a highly localized manner. Thus, it is of great importance to understand regional changes to tropical cyclone activity. Doing so, however, remains challenging, in part because changes in TC activity may be highly sensitive to the evolution of the equatorial Pacific zonal sea surface temperature (SST) gradient (Sobel et al. 2023; Lin et al. 2024; Zhao and Knutson 2024; Lin et al. 2025).

One leading hypothesis is that a long-term, multidecadal warming pattern that projects onto El Niño–Southern Oscillation (ENSO) could be understood by analogy to El Niño and La Niña events (Sobel et al. 2023). For example, SST patterns that are La Niña–like would increase Atlantic tropical cyclone activity, while SST patterns that are El Niño–like would decrease it. Since "El Niño–like" warming is modeled throughout the twenty-first century by many Coupled Model Intercomparison Project phase 6 (CMIP6) Earth system models (Cai et al. 2021), this hypothesis suggests that there will be a corresponding long-term reduction in Atlantic tropical cyclone activity throughout the twenty-first century. However, this hypothesis conflicts with the results of Fedorov et al. (2010), who found that a "permanent El Niño" during the Pliocene warm period may have been associated with a substantial increase in the frequency, strength, and poleward extent of tropical cyclones.

More recently, the hypothesis of Sobel et al. (2023) was tested in Lin et al. (2025), who found that an El Niño–like forced response over the twenty-first century was associated with a substantial El Niño–like reduction in the Atlantic tropical cyclone wind hazard. However, the physical mechanisms responsible for these changes were not investigated. An immediate question is whether it is physically consistent to use

Corresponding author: Jonathan Lin, jonathanlin@cornell.edu

DOI: 10.1175/JCLI-D-25-0536.1

the observed relationships between ENSO and Atlantic tropical cyclones as an analog for understanding how long-term patterned warming, insofar as it projects onto ENSO, affects Atlantic tropical cyclones. While El Niño and La Niña are transient events, long-term patterns of warming will elicit a more nearly equilibrated response (Chiang and Sobel 2002; Tang and Neelin 2004).

In this study, we attempt to disentangle the differences between the transient and equilibrium responses of the Atlantic to Pacific SST forcing. Section 2 outlines basic theory to understand the problem at hand. Section 3 describes the idealized double-column modeling framework used in this study. Section 4 analyzes and physically interprets both the double-column modeling results and a linear time-dependent model that approximates the double-column model. Finally, section 5 concludes this study with a summary and discussion.

2. Basic theory of the Atlantic response to Pacific SST forcing

To understand the differences between the transient and equilibrium responses of the Atlantic to Pacific SST forcing, we first consider two basins, representing the Pacific and Atlantic, in an initial radiative–convective equilibrium (RCE) state and in equilibrium with each other, as shown in Fig. 1a. The two basins are separated by a physical barrier in the ocean, and the Pacific basin is assumed to be much larger than the Atlantic. Thus, the Pacific exerts a greater control over the free-atmospheric temperature. In the initial RCE state, the boundary layer moist static energy (h_b) will be equivalent to the free-tropospheric saturation moist saturation energy (h^*), owing to boundary layer quasi equilibrium. In addition, convective quasi equilibrium in the free troposphere dictates that h^* is constant in the vertical (Arakawa and Schubert 1974).

Next, consider instantaneously imposing a positive SST anomaly in the Pacific basin, as shown in Fig. 1b, mimicking the effect of ocean heat convergence. Owing to boundary layer quasi equilibrium, the boundary layer moist static energy will rise, and the free-tropospheric saturation moist static energy will increase accordingly. The free-atmospheric h^* will evolve very quickly to radiative–convective equilibrium on the time scale of the atmospheric adjustment to the SST anomaly, which is approximately 1 month (Tompkins and Craig 1998). Now, if the Coriolis parameter were small, as is the case in the tropics, the free-tropospheric h^* would equilibrate in the horizontal, owing to weak-temperature-gradient (WTG) dynamics (Sobel and Bretherton 2000; Chiang and Sobel 2002), as shown in Fig. 1b. The Atlantic basin, where the ocean heat convergence is assumed to be zero, must then respond to the warming of the free troposphere.

We will understand the thermodynamic response of the Atlantic using both SST and potential intensity (Emanuel 1986; Bister and Emanuel 1998); note that potential intensity has been shown to accurately bound the maximum wind speed of tropical cyclones in observational data (Emanuel 2000). Since the ocean mixed layer adjustment time scale, which is around 1 year for realistic mixed layer depths, is much longer than the atmospheric

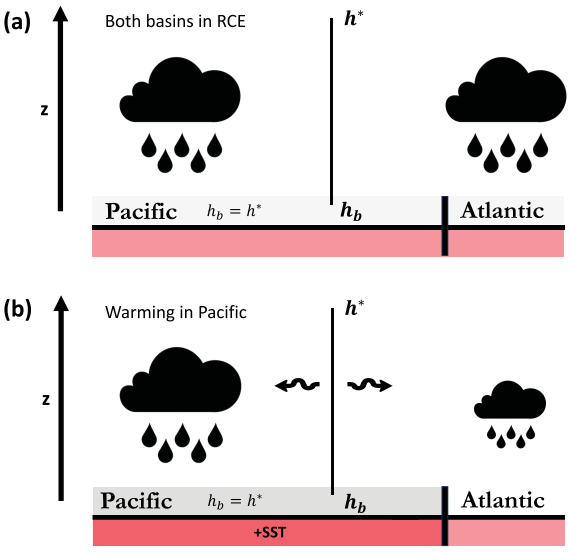

FIG. 1. Idealized schematic of two convecting columns, representing the Pacific and Atlantic basins. They are separated by a physical barrier, and the Pacific basin is much larger than the Atlantic. (a) Both the Pacific and Atlantic are in RCE, and the boundary layer moist static energy is equal to the free-tropospheric saturation moist static energy. (b) An instantaneous SST anomaly is imposed in the Pacific column, which leads to both an increase in the boundary layer moist static energy and the free-tropospheric saturation moist static energy. What is the time-dependent, thermodynamic response of the Atlantic column?

adjustment time scale (Chiang and Sobel 2002; Cronin and Emanuel 2013), the Atlantic atmospheric response to the free-tropospheric warming can be first considered as if the ocean temperature were unchanged. Owing to the warming of the free troposphere, the potential intensity in the Atlantic will initially be reduced (Tang and Neelin 2004). This can directly be seen using a saturation moist static energy formulation of potential intensity (Emanuel et al. 2013):

$$V_p^2 = \frac{C_k}{C_d}\frac{T_s - T_o}{T_o}(h_s^* - h^*), \tag{1}$$

where h_s^* is the saturation moist static energy of a surface parcel at sea surface temperature, T_s and T_o are the sea surface and tropical cyclone outflow temperatures, respectively, and C_k and C_d are the sea surface exchange coefficients for enthalpy and momentum, respectively.[1] A warming of the free troposphere without a corresponding ocean surface warming will increase h^*, while h_s^* stays constant, leading to a decrease in $(h_s^* - h^*)$. In principle, changes to the thermodynamic efficiency can also affect potential intensity. However, Sobel et al. (2019) show that changes to thermodynamic efficiency do not explain an appreciable fraction of future potential intensity

[1] In Eq. 1, the last term h^* is a proxy for the actual boundary layer moist static energy since $h^* = h_b$ in a moist neutral atmosphere.

trends in climate models. Furthermore, an increase in tropospheric temperature is likely to increase T_o, which reduces the thermodynamic efficiency and potential intensity. Hence, a decrease in $(h_s^* - h^*)$ will generally lead to a decrease in potential intensity. Therefore, the immediate transient response to Pacific warming is a reduced potential intensity in the Atlantic. Similar arguments can be made for the response of the Atlantic to Pacific cooling or La Niña events. Indeed, Atlantic potential intensity is observed to be reduced during El Niño events and elevated during La Niña events (Camargo et al. 2007).

Now let us consider the response of the Atlantic but allow the SST to evolve in time toward radiative–convective equilibrium. Over time, the Atlantic will warm owing to both reduced turbulent surface fluxes and reduced infrared cooling at the surface, as pointed out by both Chiang and Sobel (2002) and Tang and Neelin (2004). Eventually, the smaller Atlantic basin will come into thermal equilibrium, in which case the potential intensity can be written as (Emanuel 2007)

$$V_p^2 = \frac{T_s - T_o}{T_o}\frac{F_\downarrow - F_\uparrow + F_{\text{ocean}}}{C_d\rho|\mathbf{V}_s|}, \tag{2}$$

where $F_\downarrow$ is the net solar flux into the ocean, $F_\uparrow$ is the net infrared radiative flux out of the ocean, F_{ocean} is the ocean heat flux convergence, and $|\mathbf{V}_s|$ is the surface wind speed magnitude. Assuming $F_{\text{ocean}} = 0$, an unchanged surface wind speed, and negligible dependence of net solar flux on atmospheric temperature, the Atlantic equilibrium potential intensity will increase with Pacific warming because $F_\uparrow$ decreases in magnitude owing to water vapor's greenhouse effect, assuming fixed relative humidity. Then, in this simple theoretical framework, the equilibrium response in the Atlantic column is an increased potential intensity.

Therefore, the transient response of the Atlantic to Pacific SST forcing (and the consequent change to the tropical free troposphere) is of the opposite sign as its equilibrium response. This could limit the effectiveness of using El Niño/La Niña analogies to understand how long-term changes to the equatorial Pacific zonal SST gradient would alter Atlantic tropical cyclone behavior.

3. Modeling framework

To illustrate the aforementioned concept in a more quantitative framework, we use the Massachusetts Institute of Technology (MIT) single-column model (SCM) (Bony and Emanuel 2001), a one-dimensional, time-dependent system that solves equations for convective and radiative heat transfer. Moist convection is parameterized using the cumulus convection parameterization of Emanuel and Živković-Rothman (1999). Radiation is parameterized using the band-averaged radiative transfer model of Morcrette (1991) and interacts with both the surface and water vapor, though in all simulations in this study, we turn off the interaction with clouds to reduce the complexity of the model. Likewise, we specify and hold fixed vertical profiles of cloud fraction, as in Rousseau-Rizzi and Emanuel (2021). In the MIT SCM, the atmosphere can also be coupled with a slab ocean under varying mixed layer depths. This allows for the interaction between the ocean and atmosphere, which is at the core of this study. Finally, the surface wind speed is specified.

To model the idealized setup shown in Fig. 1, we couple two single columns of the MIT SCM to create a "double column" model. The first column represents the Pacific Ocean, a much bigger basin with control over the free-tropospheric temperature, and the second column represents the Atlantic Ocean. We first run both columns to RCE. The surface wind speed is set to 5 m s^{-1}, the mass concentration of CO_2 to 360 ppm, and the solar constant to 1360 W m^{-2}. The slab ocean is set to 20 m so the system evolves quickly to equilibrium. At the end of this control simulation, the SST is 300.1 K, and the potential intensity is 67.4 m s^{-1} in both columns. An SST anomaly is then imposed in the Pacific column, and we force the Atlantic column by fixing the temperature at altitudes above 850 hPa to the corresponding temperature of the Pacific column, mimicking the effects of WTG (Sobel and Bretherton 2000). To maintain energy balance in the Atlantic column, a vertical velocity is imposed at each level such that the adiabatic warming/cooling associated with this velocity exactly offsets the sum of convective and radiative heating. This vertical velocity then advects water vapor in the vertical. Finally, following Raymond and Zeng (2005), it is assumed that water vapor is entrained into the column from the "undisturbed" environment, which is assumed to be the initial RCE profile, if and only if there is horizontal convergence into the column (the entrainment term vanishes with horizontal divergence).

The time evolution of the free-tropospheric water vapor is quite important to both the transient and equilibrium solutions, as it directly modulates the surface upward infrared flux. However, a positive temperature anomaly in the Pacific can be large enough to shut off convection in the Atlantic column. Indeed, this occurs in the initial phase of all of our double-column warming simulations. The associated descent dries out the Atlantic column until the ocean warms enough for convection to restart. Thus, the free-tropospheric moisture content in the Atlantic column is modulated by convective moistening, large-scale descent, and horizontal moisture advection.

In the double-column model experiments, the control simulation is used to initialize both columns. Then, the column representing the Pacific is forced by imposing a specified SST anomaly, which is held fixed over the duration of the simulation, and the Pacific column is allowed to evolve toward equilibrium. In the Atlantic column, the surface temperature is allowed to evolve in time, and the atmospheric temperature above the boundary layer is forced to follow the temperature of the Pacific column. We run a multitude of experiments, varying both the imposed SST anomaly and the mixed layer depths to explore the parameter space of the time-dependent response of the Atlantic to Pacific SST forcing.

We stress that a key simplifying assumption here is that the area covered by the Pacific column is much larger than that covered by the Atlantic column, which is necessary to assert that the Pacific column is in RCE. In the event that the area covered by the Pacific column and the Atlantic column is

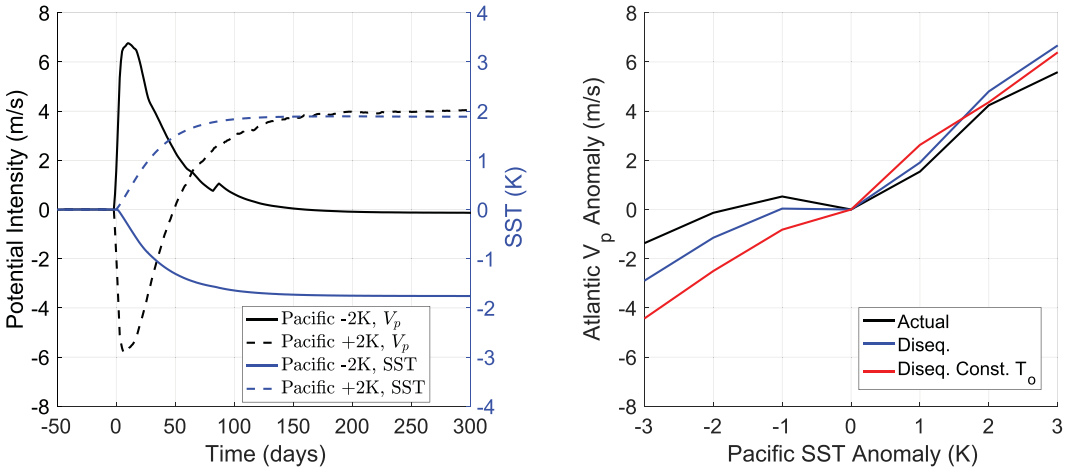

FIG. 2. (left) Time-dependent Atlantic column potential intensity (black) and SST response (blue) to an instantaneously imposed SST anomaly in the Pacific column, using a mixed layer depth of 20 m. (right) Potential intensity anomaly from the control experiment, calculated using the nonlinear CAPE-based algorithm (black), direct evaluation from Eq. (1) (blue), and direct evaluation from Eq. (1) (red) but assuming the outflow temperature is unchanged from that of the control experiment.

closer in size, any descent velocity in the Atlantic must be compensated by an ascent velocity in the Pacific column that satisfies mass conservation. In this case, neither column will be in RCE. In principle, it is possible to relax this assumption to allow one to arbitrarily specify the ratio of the areas covered by the two columns. We leave the development of a more general double-column framework to future work, which should also quantify the extent to which one can justify the Pacific column RCE approximation used in this study.

4. Results

a. *Temporal evolution of potential intensity*

Figure 2 shows the potential intensity response in the column representing the Atlantic, following the imposition of both a + 2- and a − 2-K SST anomaly in the Pacific column. The mixed layer depth in the Atlantic is set to 20 m. The results largely reflect what we intuit from theory: The Atlantic potential intensity initially decreases in response to a warming of the Pacific column, given the slow response time of the ocean. Then, over time, as the system evolves toward equilibrium, the potential intensity not only recovers but also exceeds its initial value. We note that in these experiments, the SST anomaly in the Atlantic column does not quite approach that of the Pacific (±2 K). While this effect is small, it is likely because the Pacific column is not in RCE, as the SST in the Pacific column is fixed. The Pacific itself would cool in the Pacific warming experiment since the SST is elevated above the true RCE value and vice versa for the Pacific cooling experiment.

Our experiments show that while the Atlantic transient response following Pacific cooling nearly mirrors that following Pacific warming, the equilibrium Atlantic response to −2-K Pacific cooling is near zero. Figure 2 (right) shows the equilibrium Atlantic potential intensity anomaly from the control experiment for varying Pacific SST anomalies. We observe that the equilibrium Atlantic potential intensity response is a nonlinear function of Pacific SST. Therefore, while the transient response of Atlantic potential intensity to Pacific warming is approximately linear, these results suggest that the equilibrium response cannot simply be linearized with respect to T_s (Emanuel and Sobel 2013).

To understand the causes of the differences in the equilibrium potential intensity between Pacific warming and cooling, we can evaluate the potential intensity by using Eq. (1). Figure 2 (right) shows that the potential intensity anomaly calculated from Eq. (1) reasonably follows the full nonlinear algorithm. However, when we assume a constant outflow temperature (equal to that of the control experiment) in Eq. (1), much of the nonlinearity in the Atlantic potential intensity response to Pacific SST disappears. This means that colder outflow temperatures observed in both the Pacific warming and cooling experiments are primarily responsible for the nonlinear behavior. The remaining dependence of the Atlantic potential intensity on Pacific SST must then come from either the dependence of thermodynamic efficiency on SST or the dependence of net surface radiative forcing on Pacific SST since the surface turbulent flux must be balanced by the net surface radiative forcing in equilibrium. We find that the net surface radiative forcing in the Atlantic column is approximately linear with Pacific SST (not shown). This means that, at least in the double-column model, the nonlinearity in the equilibrium Atlantic potential intensity response depends more on nonlinear changes in the outflow temperature rather than nonlinearity in the surface radiative forcing.

The observed dependence of potential intensity on outflow temperature is not entirely unrealistic, given that outflow temperatures have been documented to play a significant role in potential intensity variability (Wing et al. 2015). Furthermore, it is known that ENSO dominates the interannual variability in tropopause temperature (Gettelman et al. 2001;

Randel et al. 2009), though of course tropopause temperature is correlated with but not equivalent to the outflow temperature. However, the correlation between 500-hPa temperature and the temperature at a given layer switches sign as one moves upward through the tropical transition layer and into the lower stratosphere (Yulaeva and Wallace 1994; Grise and Thompson 2013; Lin and Emanuel 2024), so that there are large uncertainties with respect to how outflow temperature would change in response to tropospheric warming. While identifying the cause of the outflow temperature changes is beyond the scope of this work, future work should investigate whether the behavior observed in the double-column model holds true in more complex models.

It is important to understand what sets the time scale at which the potential intensity anomaly reverses sign in the Atlantic column. This time scale is determined by the equilibrium time scale for an approach to RCE with an interactive surface but specified atmospheric temperature (Cronin and Emanuel 2013):

$$\tau = \frac{H\rho_l c_l}{\rho_s C_k |\mathbf{V}_s|(c_p + L_v F)}, \tag{3}$$

where L_v is the latent heat of vaporization, c_p is the specific heat for dry air at constant pressure, and $F = (\partial q_s/\partial T)_{T_s^0}$ is evaluated using the Clausius–Clapeyron equation at a reference temperature T_s^0 (taken to be the equilibrium surface temperature in the control simulation). The reader is referred to Cronin and Emanuel (2013) and appendix A for further details. Equation (3) shows that the recovery time scale depends on the surface wind speed and is also linearly proportional to the mixed layer depth, H [as found in similar experiments performed by Chiang and Sobel (2002)]. For realistic mixed layer depths in the Atlantic main development region ($H \approx 60$ m) (de Boyer Montégut et al. 2004) and realistic surface wind speeds ($|\mathbf{V}_s| \approx 5$ m s^{-1}), we estimate that $\tau \approx 3$ months, which suggests that negative Atlantic potential intensity anomalies persist for approximately 3 months after the Pacific warms. Figure 3 verifies that the numerically estimated equilibrium time scale in the Atlantic column (obtained by fitting an exponential function to the temporal evolution of SST) roughly matches τ, consistent with the results of Cronin and Emanuel (2013).

b. Physical interpretation

The time-dependent behavior of potential intensity in the Atlantic column can be easily understood using the linear potential intensity model developed by Rousseau-Rizzi and Emanuel (2021). We rederive their model, however with changes to the physical interpretations of each term specific to the problem at hand. In the ensuing notation, all variables are anomalies unless otherwise specified. We first decompose SST perturbations into two components:

$$T_s = T_s^{\mathrm{eq}} + T_s^{\mathrm{tr}}, \tag{4}$$

where T_s^{eq} and T_s^{tr} are the equilibrium and transient Atlantic SST anomalies, respectively. In the simplified double-column

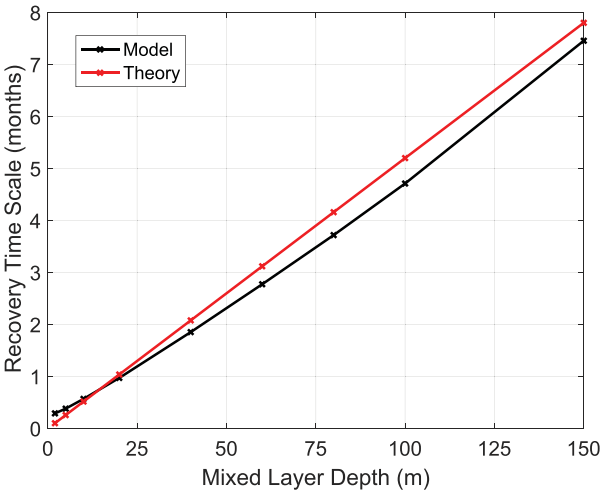

FIG. 3. Model and theory estimates of the time scale of SST evolution in the Atlantic column, under varying mixed layer depths.

experiment presented here, the equilibrium SST response is that which would be achieved when a column reaches equilibrium. In contrast, the transient response is defined as the local adjustment toward radiative–convective equilibrium, governed by WTG dynamics. We follow Rousseau-Rizzi and Emanuel (2021) by approximating the equilibrium potential intensity response to Pacific SST forcing as linear, which holds in our simulations under constant outflow temperature (see Fig. 2):

$$T_s^{\mathrm{eq}} = C_m h_m^*, \tag{5}$$

where C_m is a scaling factor that linearly relates changes in surface temperature to changes in saturation moist static energy in RCE and h_m^* is the perturbation saturation moist static energy, evaluated at midlevels. The $C_m \approx 2.6 \times 10^{-4}$ kg K J^{-1} is estimated through applying Eq. (5) to the Atlantic column simulations. Furthermore, we combine Eq. (4) and Eq. (5) to write

$$T_s^{\mathrm{tr}} = T_s - C_m h_m^*. \tag{6}$$

The transient response is thus simply equal to the actual SST change minus the SST change after the system is allowed to evolve toward equilibrium. We then apply the same decomposition to potential intensity and linearize changes to potential intensity as a function of SST:

$$V_p = V_p^{\mathrm{eq}} + V_p^{\mathrm{tr}}, \tag{7}$$

$$V_p^{\mathrm{eq}} = C_R T_s^{\mathrm{eq}}, \tag{8}$$

$$V_p^{\mathrm{tr}} = C_W T_s^{\mathrm{tr}}, \tag{9}$$

where C_R and C_W are the sensitivities of potential intensity to surface temperature in RCE and WTG, respectively, as defined in Rousseau-Rizzi and Emanuel (2021). The $C_R \approx 2.0$ m s^{-1} K^{-1} is estimated using Eq. (8), while Rousseau-Rizzi and Emanuel (2021) estimated $C_W \approx 9.0$ m s^{-1} K^{-1} from a variety of WTG

experiments. Combining Eqs. (5)–(9) yields Eq. (18) of Rousseau-Rizzi and Emanuel (2021), though with a slightly different interpretation:

$$V_p = \underbrace{C_R C_m h_m^*}_{\text{equilibrium}} + \underbrace{C_W (T_s - C_m h_m^*)}_{\text{transient}}. \tag{10}$$

From Eq. (10), it becomes clear that a positive h_m^* owing to the "global" SST forcing in the Pacific column will lead to a positive equilibrium potential intensity response in the Atlantic column. However, the transient Atlantic potential intensity response in the Atlantic is determined by a "competition" between changes in the local surface temperature (a slow time scale) and changes in the global saturation moist static energy (a relatively fast time scale). This concept is not new, as it is closely related to the idea of a disequilibrium between column stability and SST (Tang and Neelin 2004), as well as that of remote/relative SSTs (Vecchi and Soden 2007a; Latif et al. 2007; Ramsay and Sobel 2011; Camargo et al. 2013). As noted earlier, T_s evolves much slower than h_m^*, which means the transient response negatively contributes to the total potential intensity response. Given that $C_W > C_R$, the transient response dominates initially. Eventually, the system evolves toward equilibrium, $T_s = T_s^{\text{eq}}$ in the Atlantic column, such that the transient response term goes to zero, as defined in Eq. (6), and the equilibrium response term dominates.

Figure 4c (blue) compares the temporal evolution of the actual Atlantic potential intensity over time with the potential intensity change as predicted using Eq. (10) in both the Pacific warming and Pacific cooling experiments. While Eq. (10) captures the time evolution of the potential intensity in the Pacific warming case, it is less accurate in the Pacific cooling case, specifically in the equilibrium solution. As noted earlier, this is related to nonlinear changes in the outflow temperature; computing V_p assuming a constant outflow temperature reduces the equilibrium solution bias (not shown).

In these experiments, it is clear that the transient Atlantic potential intensity response to Pacific warming is opposite in sign to the equilibrium response. Importantly, the equilibrium response is tied to the global (tropical) tropospheric temperature, the free-tropospheric moisture content, and the outflow temperature. This means that warming that projects onto ENSO can only impact long-term trends in Atlantic potential intensity if the patterned warming itself modulates the tropically averaged saturation moist static energy, the deep tropospheric moisture content over the Atlantic, and/or the outflow temperature.

c. *Time-dependent linear potential intensity model*

The results in the previous section show that the Atlantic potential intensity response to Pacific SST forcing is time-dependent. Thus, it would be advantageous to transform Eq. (10) into a time-dependent model. Since potential intensity can be modeled with knowledge of just T_s and h_m^*, we can combine Eq. (10) with simple relaxation equations for h_m and T_s to model the Atlantic potential intensity response. To start, we take the time derivative of Eq. (10):

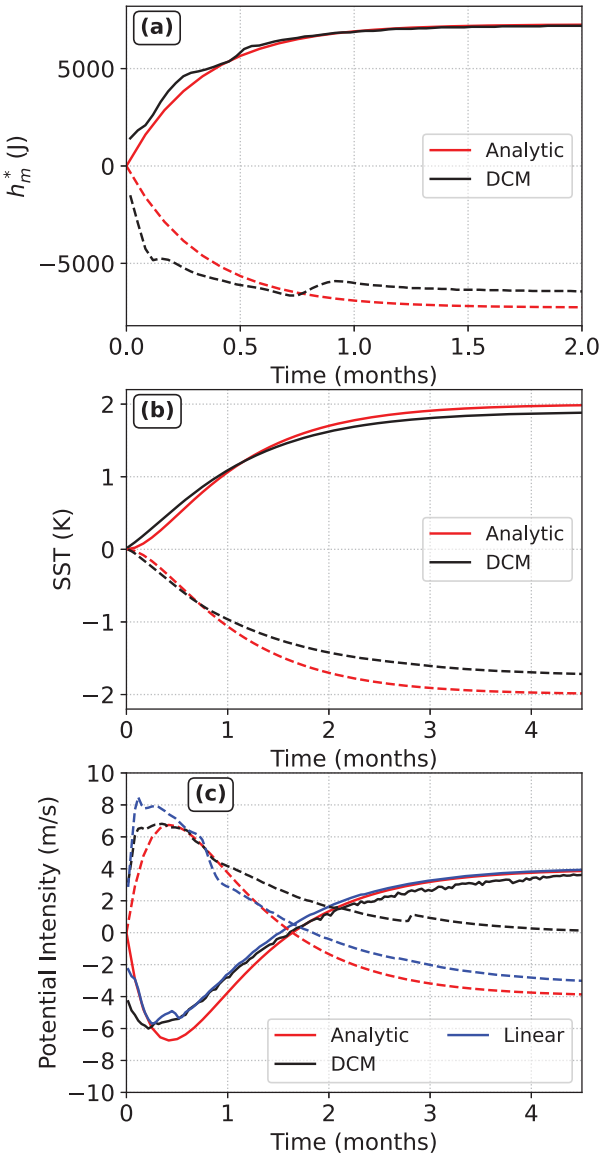

FIG. 4. (a) Time evolution of the 600-hPa saturation moist static energy in the +2-K Pacific (solid) and −2-K Pacific (dashed) experiments. Black shows h_m^* in the double-column model, while red is that in the analytic solution for $\tau_m = 10$ days [Eq. (17)]. (b) As in (a), but for SST in the Atlantic column and the analytic solution shown in Eq. (18) for $\tau_s = 25$ days. (c) As in (a), but for potential intensity in the Atlantic column and the analytic solution shown in Eq. (19). In addition, the blue line shows the potential intensity anomaly predicted by the linear state model [Eq. (10)], using $C_m = 2.6 \times 10^{-4}$ kg K J^{-1}, $C_R = 2.0$ m s^{-1} K^{-1}, and $C_W = 9.0$ m s^{-1} K^{-1}.

$$\frac{\partial V_p}{\partial t} = C_R C_m \frac{\partial h_m^*}{\partial t} + C_W \left(\frac{\partial T_s}{\partial t} - C_m \frac{\partial h_m^*}{\partial t} \right), \tag{11}$$

where h_m^* and T_s are now predictor variables. We posit that h_m^* relaxes toward its equilibrium value, defined as

$$\frac{\partial h_m^*}{\partial t} = -\frac{h_m^* - h_{m,\mathrm{eq}}^*}{\tau_m}, \tag{12}$$

where $h_{m,\mathrm{eq}}^*$ is the equilibrium value of saturation moist static energy (to be defined shortly) and τ_m is the relaxation time scale of the tropical atmosphere. We assume similar behavior for T_s:

$$\frac{\partial T_s}{\partial t} = -\frac{T_s - T_{s,\mathrm{eq}}}{\tau_s}, \tag{13}$$

where again $T_{s,\mathrm{eq}}$ is the equilibrium value and τ_s is the relaxation time scale of the ocean mixed layer. Note that τ_m and τ_s are constants.

To determine the equilibrium quantities, we linearize $h_{m,\mathrm{eq}}^*$ about a basic climatological state, with perturbations a function of the Pacific SST anomaly [see Eq. (5)]:

$$h_{m,\mathrm{eq}}^* = \frac{\delta\mathrm{SST}}{C_m}, \tag{14}$$

where δSST is the imposed SST anomaly in the Pacific column.

Consistent with the work of Chiang and Sobel (2002), we assume that WTG dynamics communicate the Pacific SST anomaly to the Atlantic via tropospheric temperature and thus determine $T_{s,\mathrm{eq}}$ using perturbations proportional to h_m^*, following Eq. (5):

$$T_{s,\mathrm{eq}} = C_m h_m^*, \tag{15}$$

where $T_{s,\mathrm{eq}}$ is also linearized about a climatological reference state. Note that $T_{s,\mathrm{eq}}$ is a function of time since h_m^* is also a function of time.

Equations (11)–(15) make up the entire linear, time-dependent system. The only inputs are the initial h_m^* and T_s anomalies (which are zero if initializing from the control), as well as the temporal evolution of the Pacific column SST anomaly, which forces the entire system. This is a dramatically simplified system that allows us to explicitly model the Pacific's modulation of SST and potential intensity in the Atlantic column [the former was first shown with realistic forcing in Chiang and Sobel (2002)].

In the idealized double-column model simulation, we have

$$\delta\mathrm{SST}(t) = AH(t), \tag{16}$$

where A is the amplitude of the SST anomaly and $H(T)$ is the Heaviside function. Assuming $h_m^*(t=0) = T_s(t=0) = V_p(t=0) = 0$, the analytic solution of the linear time-dependent system is

$$h_m^*(t) = \frac{A}{C_m}(1 - e^{-t/\tau_m}), \tag{17}$$

$$T_s(t) = \begin{cases} A\left[1 - \left(1 + \dfrac{t}{\tau}\right)e^{-t/\tau}\right], & \text{if } \tau_m = \tau_s = \tau \\ A\left(1 + \dfrac{\tau_m}{\tau_s - \tau_m}e^{-t/\tau_m} - \dfrac{\tau_s}{\tau_s - \tau_m}e^{-t/\tau_s}\right), & \text{if } \tau_m \neq \tau_s \end{cases}, \tag{18}$$

$$V_p(t) = \begin{cases} A\left[C_R - \left(C_R + \dfrac{C_{Wt}}{\tau}\right)e^{-t/\tau}\right], & \text{if } \tau_m = \tau_s = \tau \\ A\left\{\underbrace{C_R(1 - e^{-t/\tau_m})}_{\text{equilibrium}} + \underbrace{C_W\left[\left(1 + \dfrac{\tau_m}{\tau_s - \tau_m}\right)e^{-t/\tau_m} - \dfrac{\tau_s}{\tau_s - \tau_m}e^{-t/\tau_s}\right]}_{\text{transient}}\right\}, & \text{if } \tau_m \neq \tau_s \end{cases}. \tag{19}$$

For $\tau_m \neq \tau_s$, the first term in the potential intensity solution represents the approach to equilibrium, while the second term represents anomalies owing to the disequilibrium between the oceanic and atmospheric responses. This WTG term goes to zero for large t. Note that in the degenerate case of $\tau_m = \tau_s$, the solution can be attained by taking the limit of the general solution as $\tau_s \to \tau_m$.

Figure 4 shows the analytic solutions for h_m^*, T_s, and V_p to an imposed jump in Pacific SST at the initial time. We use $\tau_m = 10$ days and $\tau_s = 25$ days (the latter is consistent with the mixed layer depth of 20 m used in the Atlantic column; see Fig. 3) in the analytic solutions. We observe that the analytic solution reasonably approximates the temporal evolution of both h_m^* and T_s. Consequently, the time-dependent model also captures the temporal evolution of V_p, except for the nonlinear dependence of the equilibrium potential intensity on outflow temperature observed in the Pacific cooling experiments.

It is instructive to understand the limits of the analytic solution, as it provides us with an understanding of what controls the magnitude of the Atlantic potential intensity anomaly that is owing to Pacific SST forcing. In the limit that $\tau_m \ll \tau_s$ (the atmosphere adjustment time scale is much faster than that of the ocean), the potential intensity solution can be simplified to

$$V_p(t) = A(C_R - C_W e^{-t/\tau_s}). \tag{20}$$

This solution is simply the equilibrium potential intensity response plus a transient WTG response that decays to zero as the SST in the Atlantic approaches its equilibrium value. The potential intensity anomaly attains its maximum amplitude at $t = 0$ (when the Pacific SST anomaly is imposed) and is equal to

$$V_p(t=0) = A(C_R - C_W). \tag{21}$$

The potential intensity anomaly in the Atlantic is opposite-signed the Pacific SST anomaly (A) since $C_R < C_W$. For

the values used in the double-column model, $C_R - C_W \approx -7.0$ m s^{-1} K^{-1}, which implies that Atlantic V_p anomalies forced by Pacific SSTs can become large if there are abrupt temporal evolutions in Pacific SST, or more generally, if the Atlantic adjustment time scale is large relative to the time scale of Pacific SST change.

In the limit that $\tau_s \ll \tau_m$, the ocean adjusts much faster than the atmosphere. This regime is also analogous to a slowly varying (relative to the Atlantic Ocean adjustment time scale) Pacific SST anomaly. However, since it is not easy to modify the atmospheric adjustment time scale in the double-column model, we analyze the behavior of the analytic solution under the assumption that the linear time-dependent system approximates the double-column model for all τ_m. In this case, the temporal evolution of V_p reduces to a simple exponential approach to equilibrium:

$$V_p(t) = AC_R(1 - e^{-t/\tau_m}). \tag{22}$$

The potential intensity anomaly attains its maximum amplitude when the system reaches equilibrium ($t \to \infty$) and is

$$\max(V_p) = AC_R. \tag{23}$$

This is notably much smaller than the maximum amplitude of the V_p anomaly in the limit of $\tau_m \ll \tau_s$ [cf. to Eq. (21)] and is fundamentally related to the greater sensitivity of V_p to T_s in WTG than in RCE.

d. The Atlantic response to idealized Pacific oscillations

In the previous section, we analyzed the Atlantic potential intensity response to step functions of Pacific SST forcing. While an important exercise, there are a couple of limitations in that analysis. First, step functions in Pacific SST are highly unrealistic. Second, and more importantly, the analytic solutions assumed an initial equilibrium state. In the real world, it is possible that the Atlantic never truly reaches equilibrium with the Pacific, and thus transitory "system memory" could further modulate the magnitude of Atlantic potential intensity anomalies. As we shall see in this section, potential intensity anomalies forced by Pacific SST variability can be much larger than $A(C_R - C_W)$ for specific temporal evolutions of the Pacific SST.

To begin, we force the Pacific column with a sinusoidal SST anomaly which has a magnitude of 2 K and a period of 2 years, similar to the experiments performed in Chiang and Sobel (2002). Again, WTG is imposed in the Atlantic column. Before proceeding, we define a nondimensional time scale that is the ratio of the recovery time scale τ [Eq. (3)] to the time scale of the Pacific Ocean oscillation, τ_{Pacific}. In this case, $\tau_{\text{Pacific}} = 2$ years. We run experiments varying the mixed layer depth to explore the parameter space defined by $\tau^* = \tau/\tau_{\text{Pacific}}$. The nonlinear behavior in the equilibrium response suggests

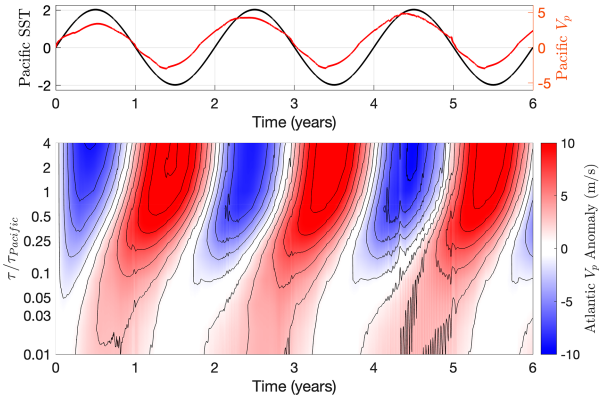

FIG. 5. (top) Temporal evolution of the SST and potential intensity anomalies in the Pacific column. (bottom) Associated temporal evolution of the potential intensity anomaly in the Atlantic column, as a function of the ratio of the recovery time scale τ [Eq. (3)] to the oscillation time scale ($\tau_{\text{Pacific}} = 2$ years).

that a sinusoidal Pacific SST forcing would produce a rectified sinusoidal potential intensity response in the Atlantic, if the Atlantic is allowed to adjust to the Pacific forcing.

Figure 5 shows the temporal evolution of the Atlantic potential intensity anomaly (with respect to the control simulation), as a function of τ^*. Indeed, the Atlantic potential intensity response to a sinusoidal Pacific forcing exhibits significant rectification. This behavior, as noted earlier, is mostly owing to an equilibrium decrease in the outflow temperature. If the nonlinearity in the outflow temperature response is indeed reflected in the real world, this suggests that the mere existence of interannual oscillations in Pacific SST—which occur in the real world because of ENSO—could cause elevated states of potential intensity in remote basins (i.e., the Atlantic) and, likely, increased tropical cyclone activity.

The magnitude of potential intensity anomalies (with respect to the mean of the rectified response) can be easily understood from the analytic solution of the time-dependent linear system under a sinusoidal SST forcing. Starting with

$$\delta\text{SST}(t) = A\,\sin(2\pi t/\tau_{\text{Pacific}}), \tag{24}$$

where τ_{Pacific} is the period of the oscillatory signal, and defining nondimensional time scales $\hat{t} = t/\tau_{\text{Pacific}}$, $\hat{\tau}_m = \tau_m/\tau_{\text{Pacific}}$, and $\hat{\tau}_s = \tau_s/\tau_{\text{Pacific}}$, we obtain

$$h_m^*(\hat{t}) = \frac{A}{C_m}\left[\frac{\sin(\hat{t}) - \hat{\tau}_m\cos(\hat{t})}{(\hat{\tau}_m^2 + 1)}\right], \tag{25}$$

$$T_s(\hat{t}) = \frac{A[(1 - \hat{\tau}_m\hat{\tau}_s)\sin(\hat{t}) - (\hat{\tau}_m + \hat{\tau}_s)\cos(\hat{t})]}{(\hat{\tau}_m^2 + 1)(\hat{\tau}_s^2 + 1)}, \tag{26}$$

$$V_p(\hat{t}) = \frac{A\{[C_R(1 + \hat{\tau}_s^2) + C_W(\hat{\tau}_m\hat{\tau}_s - \hat{\tau}_s^2)]\sin(\hat{t}) + C_W(\hat{\tau}_m\hat{\tau}_s^2 + \hat{\tau}_s)\cos(\hat{t})\}}{(\hat{\tau}_m^2 + 1)(\hat{\tau}_s^2 + 1)}. \tag{27}$$

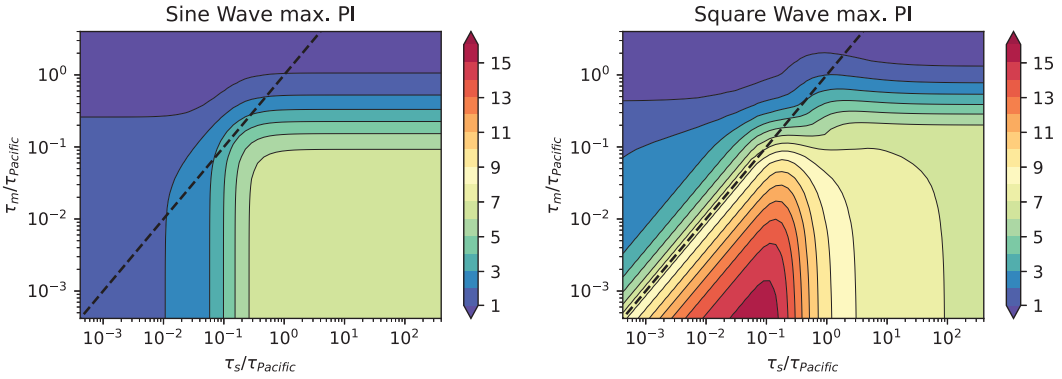

FIG. 6. (left) The maximum amplitude of the Atlantic potential intensity anomaly as a function of τ_s and τ_m, for a sinusoidal Pacific SST forcing with $A = 1$, $\tau_{\text{Pacific}} = 36$ months, $C_m = 2.6 \times 10^{-4}$ kg K J^{-1}, $C_R = 2.0$ m s^{-1} K^{-1}, and $C_W = 9.0$ m s^{-1} K^{-1}. (right) As in the left panel, but for a square wave with a period of $\tau_{\text{Pacific}} = 36$ months. Dashed black line shows $\tau_m = \tau_s$. Analytic solutions are used in the sinusoidal oscillation, and numerical solutions are used in the square wave oscillation.

The analytic potential intensity solution for the sinusoidal Pacific SST forcing nearly mirrors that obtained from the double-column simulations (Fig. B1 in appendix B), though by definition, it does not capture the rectification that occurs as a result of the nonlinearity in outflow temperature.

If the atmosphere adjusts quickly (as it does in the double-column simulations), then $V_p(\hat{t})$ simplifies to

$$\lim_{\hat{\tau}_m \to 0} V_p(\hat{t}) = AC_R \sin(\hat{t}) + \frac{AC_W[\hat{\tau}_s \cos(\hat{t}) - \hat{\tau}_s^2 \sin(\hat{t})]}{1 + \hat{\tau}_s^2}. \quad (28)$$

Unsurprisingly, in the limit where $\tau^* = \hat{\tau}_s \gg 1$, the transient response dominates, and Eq. (28) simplifies to

$$V_p(\hat{t}) = A(C_R - C_W)\sin(\hat{t}), \quad (29)$$

which shows that the Atlantic potential intensity anomaly is exactly out of phase with the Pacific SST anomaly (for $C_R < C_W$) and that the maximum anomaly magnitude matches that obtained from a similar regime in the step function forcing [Eq. (21)].

On the other hand, in the limit where the ocean adjusts quickly ($\hat{\tau}_s \ll 1$), Eq. (28) simplifies to

$$V_p(\hat{t}) = AC_R \sin(\hat{t}), \quad (30)$$

which shows that the potential intensity anomaly is exactly in phase with the Pacific SST anomaly, with a magnitude corresponding to the equilibrium sensitivity of potential intensity [Eq. (23)].

In both the $\tau^* \ll 1$ and $\tau^* \gg 1$ limits, the instantaneous Pacific SST is perfectly correlated and anticorrelated, respectively, with the instantaneous Atlantic potential intensity anomaly. However, in the intermediate regime, the potential intensity solution includes both the transient and equilibrium responses, such that the instantaneous Pacific SST no longer has a simple relationship with the Atlantic potential intensity anomaly. In other words, it is the time evolution of the Pacific SST, rather than the instantaneous Pacific SST, that is a more important determinant of the Atlantic potential intensity.

In addition, the temporal evolution of Pacific SST can strongly modulate the magnitude of the Atlantic potential intensity anomalies, beyond the $A(C_R - C_W)$ limit derived in Eq. (21). To see this clearly, we analyze the behavior of the time-dependent linear model under varying combinations of τ_s and τ_m, using two idealized Pacific SST forcings: 1) a sinusoidal oscillation (akin to the experiments just performed) and 2) a square wave forcing, defined as taking the sign of Eq. (24). We show analytic solutions for the sinusoidal oscillation and numerical solutions to the square wave oscillation.

Figure 6 shows the maximum amplitude of Atlantic potential intensity anomalies as a function of τ_s and τ_m, for a sinusoidal Pacific SST forcing with an amplitude of 1 K. There are three limits here: 1) slow atmospheric adjustment time ($\tau_m \gg \tau_{\text{Pacific}}$), 2) fast ocean and atmospheric adjustment time scales ($\tau_m \ll \tau_{\text{Pacific}}$, $\tau_s \ll \tau_{\text{Pacific}}$), and 3) slow ocean adjustment time scales ($\tau_s \gg \tau_{\text{Pacific}}$) with relatively fast atmospheric adjustment time scales. Each of these limits have been previously discussed, and the magnitudes of the maximum anomaly are 0, C_R, and $C_R - C_W$, following the arguments made above.

Interestingly, the potential intensity anomalies in the square wave SST forcing can become quite large for relatively fast atmospheric adjustment time scales when combined with oceanic adjustment time scales that are faster than the period of the square wave, as shown in Fig. 6. This behavior is not seen with a sinusoidal SST forcing. This limit can be understood by considering the time points where the square wave SST forcing transitions from A to $-A$ or at $t^* = \pi n$, where n is an integer. In the case where $\tau_s \ll \tau_{\text{Pacific}}$ and $\tau_m \ll \tau_{\text{Pacific}}$, the Atlantic state has time to equilibrate in response to SST forcing in between transitions. Then, the maximum PI will be essentially the same as that occurring in response to an instantaneous transition from an equilibrium state A to $-A$. In that case, if the ocean adjusts faster than the atmosphere ($\tau_s \ll \tau_m$), then the system should remain in near equilibrium throughout its transition from A to $-A$ despite the instantaneous change

in SST forcing, and the maximum amplitude of PI anomaly should be

$$V_p(t^* + \delta t) = AC_R. \tag{31}$$

If we continue with the case where $\tau_s \ll \tau_{\text{Pacific}}$ and $\tau_m \ll \tau_{\text{Pacific}}$ but instead consider that the atmosphere adjusts rapidly to the new forcing while the ocean varies more slowly ($\tau_s \gg \tau_m$), the disequilibrium will increase sharply leading to a large increase in PI. This can be expressed as

$$h_m^*(t^* + \delta t) = C_m h_{m,\text{eq}}^* = T_s^{\text{eq}} = -A, \tag{32}$$

$$T_s(t^* + \delta t) = A, \tag{33}$$

$$V_p(t^* + \delta t) = A(2C_W - C_R), \tag{34}$$

which shows that the maximum potential intensity anomaly magnitude equals $2C_W - C_R$ or 16 m s^{-1} K^{-1} using our estimates of C_R and C_W and greatly exceeds the limit in Eq. (21). While this behavior occurs at quite unrealistic limits, it is yet another example of how the temporal evolution of Pacific SST is important to the Atlantic potential intensity. Note also that in the case of a step function change, only the relative values of the time scales matter for determining the PI evolution shape and amplitude [see Eq. (B3)], so that for $\tau_s \ll \tau_{\text{Pacific}}$ and $\tau_m \ll \tau_{\text{Pacific}}$, the contours of maximum PI are aligned with the $\tau_s = \tau_m$ line in Fig. 6.

Finally, for adjustment time scales that are comparable to, or exceed, the forcing time scale, the PI maxima more closely resemble those of a sine wave, and in the limits where $\tau_m \gg \tau_{\text{Pacific}}$ or $\tau_s \gg \tau_{\text{Pacific}}$, we retrieve the maximum PI anomalies of 0 and $A(C_W - C_R)$, respectively.

Though the SST forcings performed in this section—steady Pacific heating and cooling, as well as perfect sinusoidal and square oscillations in Pacific SST—are highly idealized and simplified, they still exhibit complex behavior that provides better understanding of how the temporal evolution of the Pacific modulates the Atlantic potential intensity. From the above analysis, we infer that anomalously high Atlantic potential intensity states can originate from long and slow-evolving El Niño events that rapidly transition into La Niña events, and anomalously low Atlantic potential intensity states can originate from long and slow-evolving La Niña events that rapidly transition into El Niño events. Thus, the double-column model may be a useful framework to help future work further our understanding of coupled ocean–atmosphere processes in the tropics.

5. Conclusions

In this study, we aim to understand the time-dependent potential intensity response of the Atlantic to Pacific SST forcing. We first couple two single columns of the MIT SCM, each representing the Pacific and Atlantic, respectively, by setting the temperature above 850 hPa in the Atlantic column to that of the Pacific column. This has the effect of representing WTG in the tropical atmosphere (Sobel and Bretherton 2000; Chiang and Sobel 2002). We show that the transient Atlantic potential intensity response to Pacific SST forcing is opposite in sign to the equilibrium response. The basic physics can be understood from the difference in the response time scales of the (fast) atmosphere and (slow) ocean. Warming of the troposphere without corresponding changes in the ocean reduces the potential intensity. However, if the coupled ocean–atmosphere state is allowed to evolve to equilibrium, the ocean will warm (Chiang and Sobel 2002; Tang and Neelin 2004), owing to increased net surface radiative heating and reduced surface fluxes, eventually reaching a state of increased potential intensity.

We physically interpret the experiments using the linear potential intensity model of Rousseau-Rizzi and Emanuel (2021), whereby the potential intensity anomalies are decomposed into their transient and equilibrium components. We find that while the transient response, governed by WTG dynamics, is linear with respect to Pacific cooling and heating, the equilibrium response, governed by RCE dynamics, is not linear, broadly consistent with the results of Emanuel and Sobel (2013). The nonlinearity in the equilibrium response is tied to a nonlinear dependence of the outflow temperature on the Pacific column SST anomaly. Since the double-column model has a relatively limited representation of upper-tropospheric and stratospheric processes, future work should ascertain whether this behavior extends to the real world. Furthermore, in the real world, the presence of the annual cycle of solar insolation also means that the tropical Pacific and Atlantic are never truly in equilibrium. We leave further analysis of this issue to future work.

We then derive a linear, time-dependent potential intensity model, which assumes that both h_m^* and T_s linearly relax to their equilibrium values and is driven solely by the time-dependent evolution of the Pacific SST. We show that this time-dependent potential intensity model is able to accurately reproduce the Atlantic potential intensity response to both step function and sinusoidal Pacific SST forcings in the double-column framework. Analytic solutions of the linear time-dependent potential intensity model under a variety of idealized temporal evolutions of Pacific SST reveal that the temporal evolution of Pacific SST is a more important determinant of the Atlantic potential intensity than the instantaneous Pacific SST, as suggested by Tang and Neelin (2004).

The opposing signs of the transient and equilibrium potential intensity response to Pacific SST forcing bring into question the applicability of using the observed response of Atlantic tropical cyclone activity to ENSO to understand the response of Atlantic tropical cyclone activity to longer-term SST patterns of warming that project onto ENSO. Our work suggests that, unless the Pacific pattern of warming strongly controls tropical-averaged temperature and moisture, it will not have an appreciable influence on the equilibrium Atlantic potential intensity.

This conclusion may not hold if changes in surface wind speed—which could themselves be influenced by the Pacific warming pattern—also play an important role in future potential intensity trends. In RCE simulations, Emanuel and Sobel (2013)

found that changes to the surface wind speed, per unit change in SST, are by far the most important contributor to PI changes. However, Sobel et al. (2019) found that in climate models, changes to the surface wind did not explain a significant fraction of potential intensity trends, but note that this could be owing to the use of monthly mean data. Evaluating the Pacific warming pattern's influence on surface wind, as well as its subsequent effect on potential intensity, however, requires a general circulation model and will be the subject of future work.

Furthermore, while potential intensity is a necessary ingredient for tropical cyclone genesis and intensification, it is not sufficient by itself to support tropical cyclones. Indeed, much research demonstrates that ENSO's influence on vertical wind shear over the Atlantic plays a key role in modulating Atlantic tropical cyclone frequency in the region (Gray 1984; Shapiro 1987; Camargo et al. 2007). Thus, changes to vertical wind shear cannot be ignored when attempting to understand future changes to Atlantic tropical cyclone activity. While the idealized double-column framework is useful, it cannot, by definition, represent the three-dimensional circulation response to Pacific SST forcing, which has been linked to changes in Atlantic tropical cyclone activity (Vecchi and Soden 2007b). Some studies have found an increased sensitivity of tropical cyclones to vertical wind shear with increasing ocean temperature (Nolan and Rappin 2008; Emanuel 2013), and future projections have shown substantial increases in the vertical wind shear over the Atlantic basin (Vecchi and Soden 2007b; Garner et al. 2009). However, in the Atlantic basin, potential intensity has historically been anticorrelated with the vertical wind shear (Latif et al. 2007; Kossin and Vimont 2007), and thus the two may not necessarily be thought of as independent. Still, an increased understanding of the pathways through which a reduction in the equatorial Pacific zonal SST gradient influences Atlantic tropical cyclones will need to consider not only changes to the thermodynamic state (as done in this work) but also changes to the mean-state circulation.

Acknowledgments. K. Emanuel's contribution was supported through the MIT Climate Grand Challenge on Weather and Climate Extremes, with support provided by Schmidt Sciences, LLC.

Data availability statement. The MIT SCM is freely available online via https://doi.org/10.5281/zenodo.10795221 (Emanuel 2024).

APPENDIX A

Derivation of Surface Temperature in the Atlantic Column

In this section, variables are not anomalies but their absolute values. We start from the rate equation for surface temperature under a slab ocean:

$$\frac{\partial T_s}{\partial t} = \frac{F_\downarrow(t) - F_\uparrow(t) - F_{\text{surf}}(t)}{H\rho_l c_l}, \tag{A1}$$

where T_s is the mixed layer temperature, H is the mixed layer depth, ρ_l is the density of liquid water, and c_l is the heat capacity of liquid water, and F_{surf} is the turbulent surface flux out of the ocean, represented using the aerodynamic flux formula:

$$F_{\text{surf}} = \rho_s C_k |\mathbf{V}_s|(h_0^* - h_b), \tag{A2}$$

where ρ_s is the surface air density and h_0^* is the saturation moist static energy of air at the temperature of the sea surface. We assume the net solar flux into the ocean is unvarying with time. If one also makes the very rough approximation that the net surface infrared radiative flux is only a function of the free-tropospheric temperature, admitting that this will ignore changes to $F_\uparrow$ that are owing to changes in free-tropospheric moisture, $F_\uparrow$ is also not a function of time. As long as convection is active, we can also approximate $h_b \approx h^*$. However, the convective mass flux goes to zero in the Atlantic column immediately following the experiments with Pacific warming. The h_b, then, is no longer coupled to h^* and should be evaluated using the boundary layer moist static energy budget. In the spirit of simplicity, we will assume $h_b \approx h^*$ but stress that this is a poor approximation during the initial portion of the transient response.

In the special case of fixed $|\mathbf{V}_s|$, fixed free-tropospheric h^* (having already reached equilibrium in the limit under consideration), $F_\uparrow$ being only a function of h^* and $h_b \approx h^*$, such that F_{surf} becomes only a function of h_0^*, which itself is a (nonlinear) function of T_s. Under these simplifications, the mixed layer temperature tendency equation becomes

$$\frac{\partial T_s}{\partial t} = \frac{F_\downarrow - F_\uparrow - \rho_s C_k |\mathbf{V}_s|[h_0^*(T_s) - h^*]}{H\rho_l c_l}, \tag{A3}$$

where $F_\downarrow$ and $F_\uparrow$ are assumed to have reached their equilibrium values. For Pacific column SST anomalies small in magnitude, we can linearize the dependence of h_0^* on T_s.

To do this, we linearize the surface saturation specific humidity about the base-state surface temperature:

$$q_s(T_s) = q_s^0 + \left(\frac{\partial q_s}{\partial T}\right)_{T_s^0}(T_s - T_s^0), \tag{A4}$$

where q_s is the surface saturation specific humidity, T_s^0 is the reference surface temperature, and q_s^0 is the saturation specific humidity at the reference surface temperature. Note that $F = (\partial q_s/\partial T)_{T_s^0}$ is evaluated using the Clausius–Clapeyron equation. Then, we can define the surface saturation moist static energy as

$$h_0^*(T_s) = c_p T_s + L_v q_s(T_s). \tag{A5}$$

Substituting Eq. (A5) into Eq. (A3) and simplifying yields

$$\frac{\partial T_s}{\partial t} = \underbrace{\frac{F_\downarrow - F_\uparrow + \rho_s C_k |\mathbf{V}_s|[h^* - L_v(q_s^0 - FT_s^0)]}{H\rho_l c_l}}_{\alpha} - \underbrace{\frac{\rho_s C_k |\mathbf{V}_s|(c_p + L_v F)}{H\rho_l c_l}}_{1/\tau} T_s, \tag{A6}$$

which has the general solution:

$$T_s(t) = \alpha\tau + (T^* - \alpha\tau)\exp\left(-\frac{t}{\tau}\right), \tag{A7}$$

where $T^* = T_s(t = 0)$. In our estimates of τ, $C_k = 1 \times 10^{-3}$, $L_v = 2.5 \times 10^6$ J kg^{-1}, $c_p = 1005$ J (kg K)$^{-1}$, $c_l = 4160$ J (kg K)$^{-1}$, $\rho_s = 1.225$ kg m^{-3}, and $\rho_l = 1000$ kg m^{-3}.

APPENDIX B

Analytic Solutions of the Time-Dependent Model

a. Sinusoidal Pacific SST forcing

The analytic solution [Eq. (27)] of the Atlantic potential intensity anomaly under a 2-yr sinusoidal Pacific SST forcing is shown in Fig. B1. The analytic solution reproduces the double-column model response, except for the rectification that occurs as a result of nonlinearity in the outflow temperature.

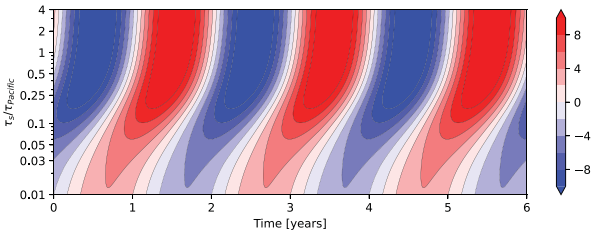

FIG. B1. Analytic solution [Eq. (27)] of the Atlantic potential intensity anomaly under a 2-yr sinusoidal Pacific SST forcing, for varying mixed layer depth time scales. Compare with Fig. 5.

b. Step functions from A to −A

Here, we consider the analytic solution of the time-dependent potential intensity model under a step function in SST forcing from A to $-A$. The analytic solution is

$$h_m^*(t) = \frac{A}{C_m}(2e^{-t/\tau_m} - 1), \tag{B1}$$

$$T_s(t) = \begin{cases} A\left[1 + 2\left(1 + \dfrac{t}{\tau}\right)e^{-t/\tau}\right], & \text{if } \tau_m = \tau_s = \tau \\ A\left(2\dfrac{\tau_s}{\tau_s - \tau_m}e^{-t/\tau_s} - 2\dfrac{\tau_m}{\tau_s - \tau_m}e^{-t/\tau_m} - 1\right), & \text{if } \tau_m \neq \tau_s \end{cases}, \tag{B2}$$

$$V_p(t) = \begin{cases} A\left[-C_R + 2\left(C_R + \dfrac{C_{W'}}{\tau}\right)e^{-t/\tau}\right], & \text{if } \tau_m = \tau_s = \tau \\ A\left[\underbrace{C_R(2e^{-t/\tau_m} - 1)}_{\text{equilibrium}} + \underbrace{2C_W\dfrac{\tau_s}{\tau_s - \tau_m}(e^{-t/\tau_m} - e^{-t/\tau_s})}_{\text{transient}}\right], & \text{if } \tau_m \neq \tau_s \end{cases}. \tag{B3}$$

REFERENCES

Arakawa, A., and W. H. Schubert, 1974: Interaction of a cumulus cloud ensemble with the large-scale environment, Part I. *J. Atmos. Sci.*, **31**, 674–701, https://doi.org/10.1175/1520-0469(1974)031<0674:IOACCE>2.0.CO;2.

Balaguru, K., and Coauthors, 2023: Increased U.S. coastal hurricane risk under climate change. *Sci. Adv.*, **9**, eadf0259, https://doi.org/10.1126/sciadv.adf0259.

Bister, M., and K. A. Emanuel, 1998: Dissipative heating and hurricane intensity. *Meteor. Atmos. Phys.*, **65**, 233–240, https://doi.org/10.1007/BF01030791.

Bony, S., and K. A. Emanuel, 2001: A parameterization of the cloudiness associated with cumulus convection; evaluation using TOGA COARE data. *J. Atmos. Sci.*, **58**, 3158–3183, https://doi.org/10.1175/1520-0469(2001)058<3158:APOTCA>2.0.CO;2.

Cai, W., and Coauthors, 2021: Changing El Niño–Southern Oscillation in a warming climate. *Nat. Rev. Earth Environ.*, **2**, 628–644, https://doi.org/10.1038/s43017-021-00199-z.

Camargo, S. J., K. A. Emanuel, and A. H. Sobel, 2007: Use of a genesis potential index to diagnose ENSO effects on tropical cyclone genesis. *J. Climate*, **20**, 4819–4834, https://doi.org/10.1175/JCLI4282.1.

——, M. Ting, and Y. Kushnir, 2013: Influence of local and remote SST on North Atlantic tropical cyclone potential intensity. *Climate Dyn.*, **40**, 1515–1529, https://doi.org/10.1007/s00382-012-1536-4.

Chiang, J. C. H., and A. H. Sobel, 2002: Tropical tropospheric temperature variations caused by ENSO and their influence on the remote tropical climate. *J. Climate*, **15**, 2616–2631, https://doi.org/10.1175/1520-0442(2002)015<2616:TTTVCB>2.0.CO;2.

Cronin, T. W., and K. A. Emanuel, 2013: The climate time scale in the approach to radiative-convective equilibrium. *J. Adv. Model. Earth Syst.*, **5**, 843–849, https://doi.org/10.1002/jame.20049.

de Boyer Montégut, C., G. Madec, A. S. Fischer, A. Lazar, and D. Iudicone, 2004: Mixed layer depth over the global ocean: An examination of profile data and a profile-based climatology. *J. Geophys. Res.*, **109**, C12003, https://doi.org/10.1029/2004JC002378.

Emanuel, K., 2000: A statistical analysis of tropical cyclone intensity. *Mon. Wea. Rev.*, **128**, 1139–1152, https://doi.org/10.1175/1520-0493(2000)128<1139:ASAOTC>2.0.CO;2.

——, 2007: Environmental factors affecting tropical cyclone power dissipation. *J. Climate*, **20**, 5497–5509, https://doi.org/10.1175/2007JCLI1571.1.

——, 2021: Response of global tropical cyclone activity to increasing CO_2: Results from downscaling CMIP6 models. *J. Climate*, **34**, 57–70, https://doi.org/10.1175/JCLI-D-20-0367.1.

——, 2024: FORTRAN Program and MATLAB analysis scripts for single-column model. Zenodo, https://doi.org/10.5281/zenodo.10795222.

——, and A. Sobel, 2013: Response of tropical sea surface temperature, precipitation, and tropical cyclone-related variables to changes in global and local forcing. *J. Adv. Model. Earth Syst.*, **5**, 447–458, https://doi.org/10.1002/jame.20032.

——, S. Solomon, D. Folini, S. Davis, and C. Cagnazzo, 2013: Influence of tropical tropopause layer cooling on Atlantic hurricane activity. *J. Climate*, **26**, 2288–2301, https://doi.org/10.1175/JCLI-D-12-00242.1.

Emanuel, K. A., 1986: An air-sea interaction theory for tropical cyclones. Part I: Steady-state maintenance. *J. Atmos. Sci.*, **43**, 585–605, https://doi.org/10.1175/1520-0469(1986)043<0585:AASITF>2.0.CO;2.

——, 1987: The dependence of hurricane intensity on climate. *Nature*, **326**, 483–485, https://doi.org/10.1038/326483a0.

——, 2013: Downscaling CMIP5 climate models shows increased tropical cyclone activity over the 21st century. *Proc. Natl. Acad. Sci. USA*, **110**, 12 219–12 224, https://doi.org/10.1073/pnas.1301293110.

——, and M. Živković-Rothman, 1999: Development and evaluation of a convection scheme for use in climate models. *J. Atmos. Sci.*, **56**, 1766–1782, https://doi.org/10.1175/1520-0469(1999)056<1766:DAEOAC>2.0.CO;2.

Fedorov, A. V., C. M. Brierley, and K. Emanuel, 2010: Tropical cyclones and permanent El Niño in the early Pliocene epoch. *Nature*, **463**, 1066–1070, https://doi.org/10.1038/nature08831.

Garner, S. T., I. M. Held, T. Knutson, and J. Sirutis, 2009: The roles of wind shear and thermal stratification in past and projected changes of Atlantic tropical cyclone activity. *J. Climate*, **22**, 4723–4734, https://doi.org/10.1175/2009JCLI2930.1.

Gettelman, A., W. J. Randel, S. Massie, F. Wu, W. G. Read, and J. M. Russell III, 2001: El Niño as a natural experiment for studying the tropical tropopause region. *J. Climate*, **14**, 3375–3392, https://doi.org/10.1175/1520-0442(2001)014<3375:ENOAAN>2.0.CO;2.

Gray, W. M., 1984: Atlantic seasonal hurricane frequency. Part I: El Niño and 30 mb Quasi-Biennial Oscillation influences. *Mon. Wea. Rev.*, **112**, 1649–1668, https://doi.org/10.1175/1520-0493(1984)112<1649:ASHFPI>2.0.CO;2.

Grise, K. M., and D. W. J. Thompson, 2013: On the signatures of equatorial and extratropical wave forcing in tropical tropopause layer temperatures. *J. Atmos. Sci.*, **70**, 1084–1102, https://doi.org/10.1175/JAS-D-12-0163.1.

Knutson, T., and Coauthors, 2020: Tropical cyclones and climate change assessment: Part II: Projected response to anthropogenic warming. *Bull. Amer. Meteor. Soc.*, **101**, E303–E322, https://doi.org/10.1175/BAMS-D-18-0194.1.

Kossin, J. P., and D. J. Vimont, 2007: A more general framework for understanding Atlantic hurricane variability and trends. *Bull. Amer. Meteor. Soc.*, **88**, 1767–1782, https://doi.org/10.1175/BAMS-88-11-1767.

Latif, M., N. Keenlyside, and J. Bader, 2007: Tropical sea surface temperature, vertical wind shear, and hurricane development. *Geophys. Res. Lett.*, **34**, L01710, https://doi.org/10.1029/2006GL027969.

Lin, J., and K. Emanuel, 2024: Tropospheric thermal forcing of the stratosphere through quasi-balanced dynamics. *J. Atmos. Sci.*, **81**, 561–582, https://doi.org/10.1175/JAS-D-23-0081.1.

——, C.-Y. Lee, S. J. Camargo, and A. Sobel, 2024: Poleward migration of the latitude of maximum tropical cyclone intensity—Forced or natural? *J. Climate*, **37**, 5453–5463, https://doi.org/10.1175/JCLI-D-23-0705.1.

——, ——, ——, A. H. Sobel, and J.-Y. Zhuo, 2025: The response of tropical cyclone hazard to natural and forced patterns of warming. *npj Climate Atmos. Sci.*, **8**, 109, https://doi.org/10.1038/s41612-025-00997-y.

Mendelsohn, R., K. Emanuel, S. Chonabayashi, and L. Bakkensen, 2012: The impact of climate change on global tropical cyclone damage. *Nat. Climate Change*, **2**, 205–209, https://doi.org/10.1038/nclimate1357.

Morcrette, J.-J., 1991: Radiation and cloud radiative properties in the European Centre for Medium Range Weather Forecasts forecasting system. *J. Geophys. Res.*, **96**, 9121–9132, https://doi.org/10.1029/89JD01597.

Nolan, D. S., and E. D. Rappin, 2008: Increased sensitivity of tropical cyclogenesis to wind shear in higher SST environments. *Geophys. Res. Lett.*, **35**, L14805, https://doi.org/10.1029/2008GL034147.

Ramsay, H. A., and A. H. Sobel, 2011: Effects of relative and absolute sea surface temperature on tropical cyclone potential intensity using a single-column model. *J. Climate*, **24**, 183–193, https://doi.org/10.1175/2010JCLI3690.1.

Randel, W. J., R. R. Garcia, N. Calvo, and D. Marsh, 2009: ENSO influence on zonal mean temperature and ozone in the tropical lower stratosphere. *Geophys. Res. Lett.*, **36**, L15822, https://doi.org/10.1029/2009GL039343.

Raymond, D. J., and X. Zeng, 2005: Modelling tropical atmospheric convection in the context of the weak temperature gradient approximation. *Quart. J. Roy. Meteor. Soc.*, **131**, 1301–1320, https://doi.org/10.1256/qj.03.97.

Rousseau-Rizzi, R., and K. Emanuel, 2021: A weak temperature gradient framework to quantify the causes of potential intensity variability in the tropics. *J. Climate*, **34**, 8669–8682, https://doi.org/10.1175/JCLI-D-21-0139.1.

Sarhadi, A., R. Rousseau-Rizzi, K. Mandli, J. Neal, M. P. Wiper, M. Feldmann, and K. Emanuel, 2024: Climate change contributions to increasing compound flooding risk in New York City. *Bull. Amer. Meteor. Soc.*, **105**, E337–E356, https://doi.org/10.1175/BAMS-D-23-0177.1.

Shapiro, L. J., 1987: Month-to-month variability of the Atlantic tropical circulation and its relationship to tropical storm formation. *Mon. Wea. Rev.*, **115**, 2598–2614, https://doi.org/10.1175/1520-0493(1987)115<2598:MTMVOT>2.0.CO;2.

Sobel, A. H., and C. S. Bretherton, 2000: Modeling tropical precipitation in a single column. *J. Climate*, **13**, 4378–4392, https://doi.org/10.1175/1520-0442(2000)013<4378:MTPIAS>2.0.CO;2.

——, S. J. Camargo, and M. Previdi, 2019: Aerosol versus greenhouse gas effects on tropical cyclone potential intensity and the hydrologic cycle. *J. Climate*, **32**, 5511–5527, https://doi.org/10.1175/JCLI-D-18-0357.1.

——, and Coauthors, 2023: Near-term tropical cyclone risk and coupled Earth system model biases. *Proc. Natl. Acad. Sci. USA*, **120**, e2209631120, https://doi.org/10.1073/pnas.2209631120.

Tang, B. H., and J. D. Neelin, 2004: ENSO influence on Atlantic hurricanes via tropospheric warming. *Geophys. Res. Lett.*, **31**, L24204, https://doi.org/10.1029/2004GL021072.

Tompkins, A. M., and G. C. Craig, 1998: Time-scales of adjustment to radiative-convective equilibrium in the tropical atmosphere.

Quart. J. Roy. Meteor. Soc., **124**, 2693–2713, https://doi.org/10.1002/qj.49712455208.

Vecchi, G. A., and B. J. Soden, 2007a: Effect of remote sea surface temperature change on tropical cyclone potential intensity. *Nature*, **450**, 1066–1070, https://doi.org/10.1038/nature06423.

——, and ——, 2007b: Increased tropical Atlantic wind shear in model projections of global warming. *Geophys. Res. Lett.*, **34**, L08702, https://doi.org/10.1029/2006GL028905.

Wing, A. A., K. Emanuel, and S. Solomon, 2015: On the factors affecting trends and variability in tropical cyclone potential intensity. *Geophys. Res. Lett.*, **42**, 8669–8677, https://doi.org/10.1002/2015GL066145.

Yulaeva, E., and J. M. Wallace, 1994: The signature of ENSO in global temperature and precipitation fields derived from the microwave sounding unit. *J. Climate*, **7**, 1719–1736, https://doi.org/10.1175/1520-0442(1994)007<1719:TSOEIG>2.0.CO;2.

Zhang, Q., L. Wu, and Q. Liu, 2009: Tropical cyclone damages in China 1983–2006. *Bull. Amer. Meteor. Soc.*, **90**, 489–496, https://doi.org/10.1175/2008BAMS2631.1.

Zhao, M., and T. Knutson, 2024: Crucial role of sea surface temperature warming patterns in near-term high-impact weather and climate projection. *npj Climate Atmos. Sci.*, **7**, 130, https://doi.org/10.1038/s41612-024-00681-7.